High Energy Density Physics 8 (2012) 141–149

Contents lists available at SciVerse ScienceDirect

High Energy Density Physics

journal homepage: www.elsevier.com/locate/hedp

Simulations of laser experiments of radiative and non-radiative shocks

B. Fryxell*, E. Rutter, E.S. Myra

University of Michigan, AOSS, 2455 Hayward St., Ann Arbor, MI 48109-2413, USA

ARTICLE INFO

Article history:
Received 8 December 2011
Accepted 8 December 2011
Available online 16 December 2011

Keywords:
High energy density physics
Laser astrophysics
Radiation-hydrodynamics
Shocks

ABSTRACT

The Center for Radiative Shock Hydrodynamics (CRASH) at the University of Michigan was established to study the properties of radiative shocks using both numerical simulation and shock-tube experiments on the Omega Laser at the University of Rochester. The laser accelerates a thin Be disk, which acts like a piston, driving a shock with an initial propagation velocity of 200 km/s into a tube filled with Xe. Analytic estimates indicate that a shock propagating with a velocity greater than about 60 km/s through Xe under these conditions should be strongly radiative. This paper discusses numerical simulations of a proposed modification to this experiment that produces a non-radiative shock. Comparison of the radiative and non-radiative cases provides an excellent opportunity for assessing the effects of radiation on shock structure and flow morphology. For the non-radiative case, the initial shock speed is reduced to 20 km/s by increasing the thickness of the Be disk and by decreasing the energy of the laser. Two-dimensional simulations of targets with cylindrical shock tubes and three-dimensional simulations of more complex targets with elliptical shock tubes are described. In addition, the effect of the shock speed on the cross-sectional area of the tube is discussed.

1. Introduction

The structure of shocks propagating at sufficiently large velocities can be significantly modified by radiation. For simple hydrodynamic shocks in monatomic gases, compression is limited to a factor of four. This is not true for radiative shocks, where compressions of 25 or more can easily be obtained. Studying the physics of radiative shocks is important for understanding many astrophysical environments, including supernova explosions [1], supernova remnants [2–4], and accretion flows [5]. Their complex structure presents significant challenges for numerical simulation, making code validation by laboratory experiment a necessity. The Center for Radiative Shock Hydrodynamics (CRASH) was established at the University of Michigan by the United States Department of Energy to improve our understanding of these shocks through the use of both laboratory experiments and numerical simulations. As a further step toward understanding these shocks, we have proposed a modification to the baseline CRASH experiment in which the shock is non-radiative. Comparison of the radiative and non-radiative cases provides an excellent opportunity to assess the effects of radiation on shock structure and flow morphology. This paper describes numerical simulations of the proposed non-radiative experiments and discusses differences between the radiative and non-radiative cases.

The design of the non-radiative experiment requires producing a slower shock. The energy flux advected into a shock is given by $\rho u_s^3/2$, where ρ is the pre-shock density and u_s is the shock speed. The energy flux radiated out of the shock is σT^4, where σ is the Stefan–Boltzmann constant, and T is the post-shock temperature. From the Rankine–Hugoniot relations, it is easy to determine that the post-shock temperature is proportional to the square of the shock speed for a strong, simple hydrodynamic shock. Thus the ratio of radiative energy flux to advected energy flux is proportional to u_s^5, providing a very steep transition between hydrodynamic and radiative shocks. For the parameters in our experiments, the shock is predicted to be radiative at speeds greater than 60 km/s. For more details on radiative shocks in our context see Drake et al. [6].

The remainder of the paper is organized as follows. Section 2 describes the laboratory experiments for both the radiative and non-radiative cases. The numerical codes used to simulate the experiments are described briefly in Section 3. In Section 4, we compare simulation results for radiative and non-radiative experiments and describe simulations of possible future experiments using more complex targets. Finally, in Section 5, we summarize the major findings of this work.

2. Description of laboratory experiments

Radiative shocks can be generated in the laboratory using a variety of techniques, as described in [6] and references therein.

* Corresponding author.
E-mail address: fryxell@umich.edu (B. Fryxell).

1574-1818/$ – see front matter © 2011 Elsevier B.V. All rights reserved.
doi:10.1016/j.hedp.2011.12.002

The CRASH baseline experiment uses a shock tube with energy provided by a high-power laser. The target consists of a 20 μm thick Be disk attached to a polyimide tube 600 μm in diameter and approximately 4 mm in length filled with Xe gas at a pressure slightly more than 1 atm. The initial mass density of Xe is approximately 0.0065 g/cm^3. The tube prevents the shock from expanding, weakening, and slowing to the point that it becomes non-radiative. The experiments described were performed using the Omega Laser at the Laboratory for Laser Energetics at the University of Rochester. Ten beams of the laser strike the Be disk with a total energy of 3.8 kJ. The laser pulse has a duration of 1 ns, a wavelength of 0.35 μm and covers a spot ~800 μm in diameter. The initial pressure in the Be is approximately 50 Mbars. The disk is accelerated and acts as a piston, driving a strong shock into the Xe. The shock breaks out of the Be at approximately 0.5 ns and reaches an initial speed of approximately 200 km/s, which is well into the radiative regime. The shock decelerates somewhat during the experiment, but always remains will above the radiative threshold.

The primary diagnostic used for these experiments is X-ray radiography. Additional laser beams strike a thin foil producing X-rays that pass through a pinhole to produce an image, usually on film. Images have been obtained at times ranging from 13 to 26 ns. A schematic diagram of the CRASH baseline experiment is show in Fig. 1.

The proposed non-radiative version of the experiment is nearly identical to the radiative case. Two changes are required to reduce the shock speed into the non-radiative regime. First, the laser energy is reduced from 3.8 kJ to 1.0 kJ, providing less of an impulse to the Be disk. Second, the thickness of the Be disk is increased from 20 μm to 200 μm, giving the laser more mass to accelerate. The initial shock speed resulting from these two changes is reduced to ~20 km/s, well below the radiative threshold. The simplest version of the experiment uses a straight, cylindrical shock tube with diameter increased from 600 μm to 1200 μm. A more complicated version connects the 1200 μm diameter tube to a 600 μm diameter tube using either a nozzle or a step. These three configurations are illustrated in Fig. 2. This figure also illustrates the five materials used in current simulations: the Be disk, the shock tube wall made of polyimide, the Xe gas within the shock tube, a gold washer used to prevent the shock from propagating into the region outside the tube, and the inner edge of an acrylic cone used to shield the diagnostic from stray radiation. A still more complicated option being considered for future experiments is to replace the small-diameter section of the tube with an elliptical tube having major axes of 600 μm and 1200 μm. Again, the elliptical tube would be connected to the circular tube using either a nozzle or a step (see Fig. 3). In this case, the flow is inherently three dimensional.

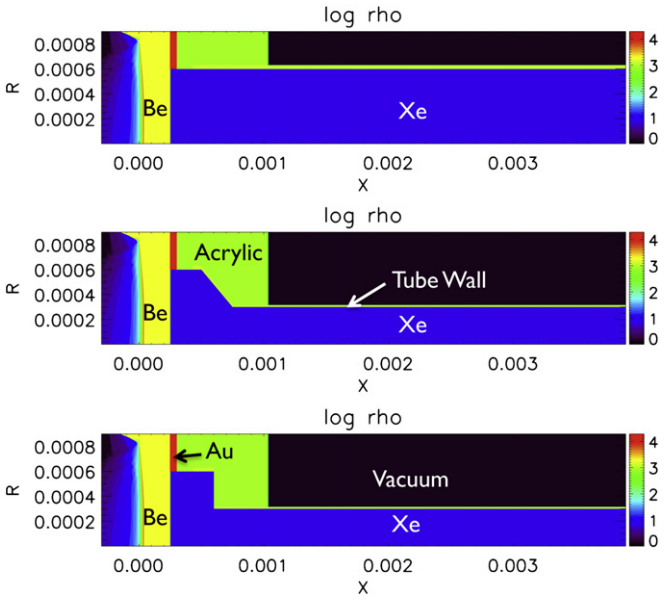

Fig. 2. Three possible configurations for future targets using a large-diameter, straight, cylindrical shock tube (top), and a large-diameter, cylindrical shock tube connected to a small-diameter, cylindrical tube by either a nozzle (middle) or a step (bottom). Only the top half of the targets are shown; the configurations are cylindrically symmetric about the bottom axis.

3. Simulation codes

We require two simulation codes to model the experiments described in the previous section. The early evolution up to time 1.1 ns is computed using Hyades [7], a two-dimensional radiation-

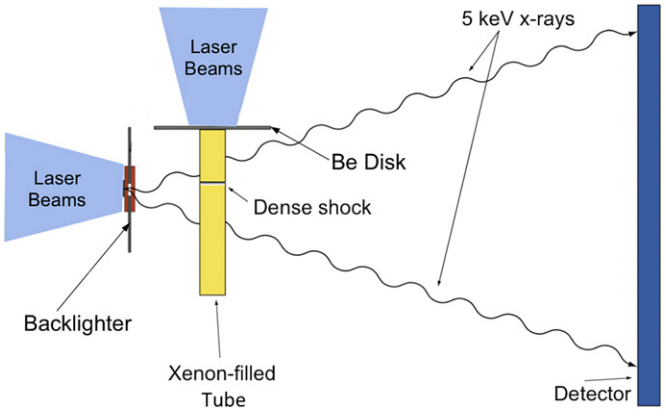

Fig. 1. Diagram showing the target geometry for the baseline CRASH experiment. The target consists of a 20 μm thick Be disk fastened to a polyimide tube filled with Xe gas. The disk is accelerated by a laser and drives a radiative shock into the Xe. The main diagnostic is an X-ray backlighter, which consists of a thin foil illuminated by additional laser beams to produce X-rays that produce a picture on film using pinhole imaging.

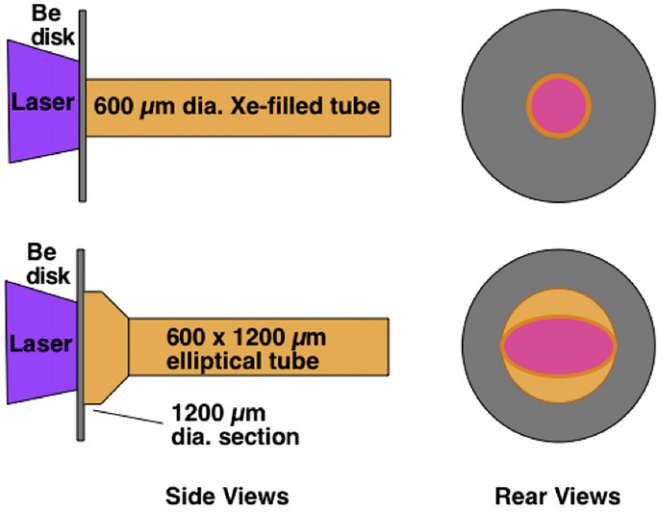

Fig. 3. Target configurations using a straight cylindrical tube (top) and a cylindrical tube connected to an elliptical tube by a nozzle (bottom). The cross section of the shock tube is depicted by the pink region in the rear views.

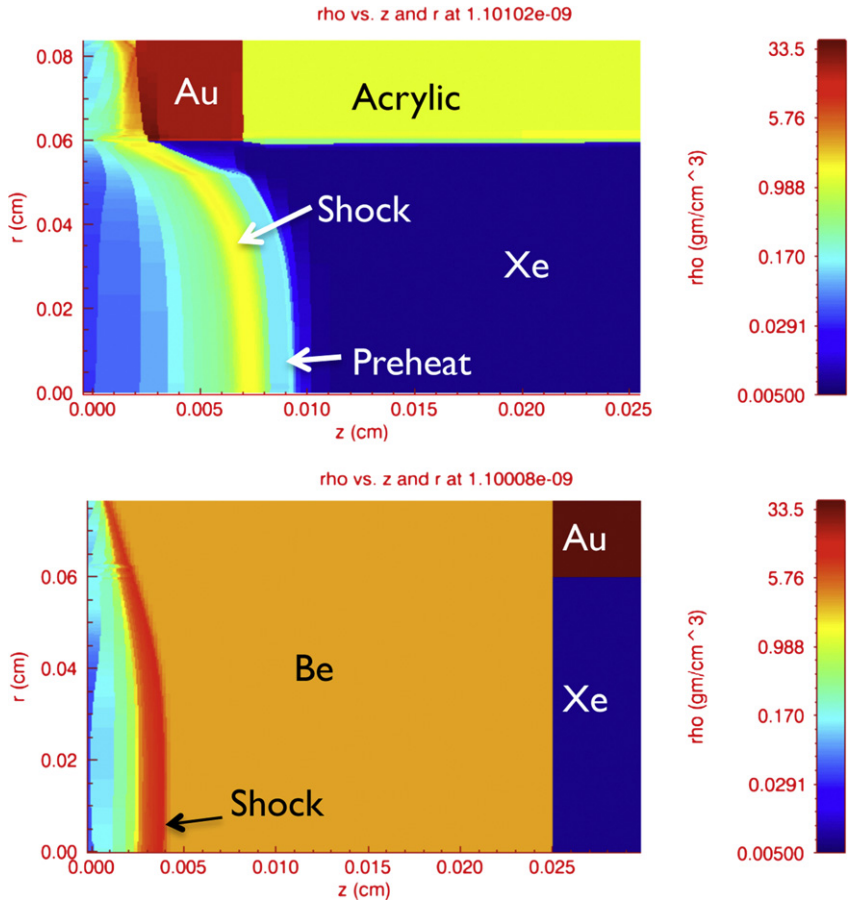

Fig. 4. Density at 1.1 ns obtained from two-dimensional Hyades simulations for the radiative case (top) and non-radiative case (bottom). The calculations are cylindrically symmetric about the bottom axis. For the radiative case, the shock has broken out of the Be into the Xe at this time, and the radiation preheat ahead of the shock is apparent. For the non-radiative case, the shock is still well within the Be disk and there is no preheat ahead of the shock, since without radiation, no signal can propagate ahead of the shock.

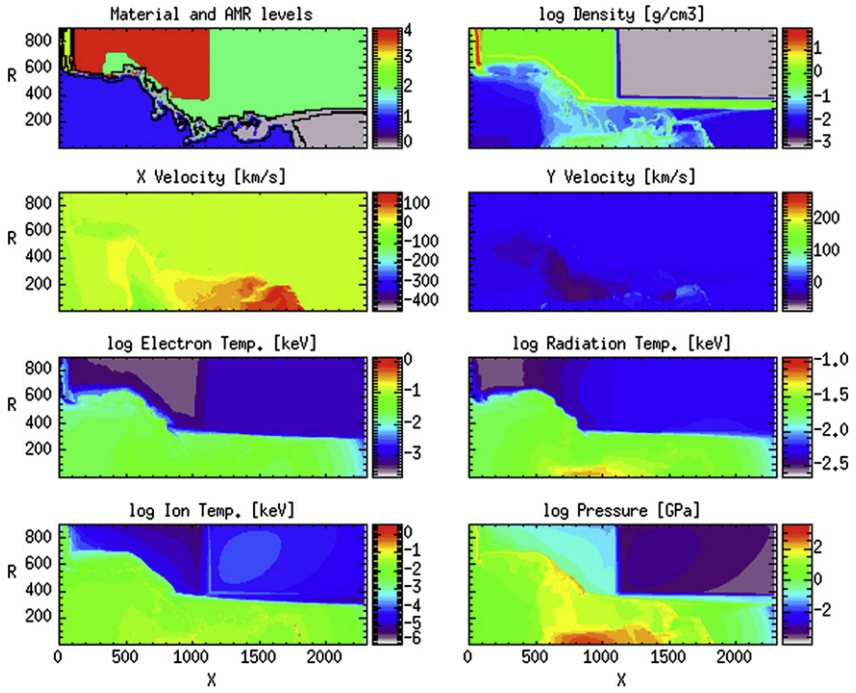

Fig. 5. Results at 13 ns from a two-dimensional, cylindrically-symmetric CRASH simulation of the radiative case for a target containing a nozzle. The plots in the left column (from top to bottom) show AMR level contours and the regions of the grid occupied by each material, horizontal component of velocity, electron temperature, and ion temperature. The right column shows density, vertical component of velocity, radiation temperature, and total pressure. The location of the primary shock and wall shock are illustrated on the plot of density.

hydrodynamics code. The code solves Lagrange's equations for compressible, inviscid gas dynamics coupled to a flux-limited, multigroup radiative transfer solver. Flux-limited electron heat conduction is also included. The electrons, ions, and radiation are each allowed to have different temperatures. Equations of state and opacity data for each of the five materials used in the experiment are read from tables. Hyades also includes a module to compute the laser–plasma interaction. However, Hyades has difficulty simulating the late-time evolution as a result of grid tangling frequently encountered when computing complex flows with Lagrangian codes. A limited automatic rezoning capability has been added to the code to allow the calculation to continue to later times, but when that fails, a manual rezoning procedure is required. This is a very labor-intensive process not practical for the large number of simulations we need to carry out. In addition, the required three-dimensional simulations of future experiments are beyond the capabilities of Hyades.

The output from Hyades at 1.1 ns is interpolated onto a Cartesian grid and used as input to CRASH [8], a three-dimensional Eulerian radiation-hydrodynamics code that contains all the physics necessary to simulate the experiments except for a laser package. For this reason, CRASH cannot be used to compute the early evolution of the system and can be used only after the laser turns off. It solves Euler's equations for compressible gas dynamics, uses either a gray or multigroup flux-limited diffusion solver for radiation transfer, contains a flux-limited electron heat conduction solver, and allows different temperatures for electrons, ions, and radiation. Equations of state and opacities for each material are pre-

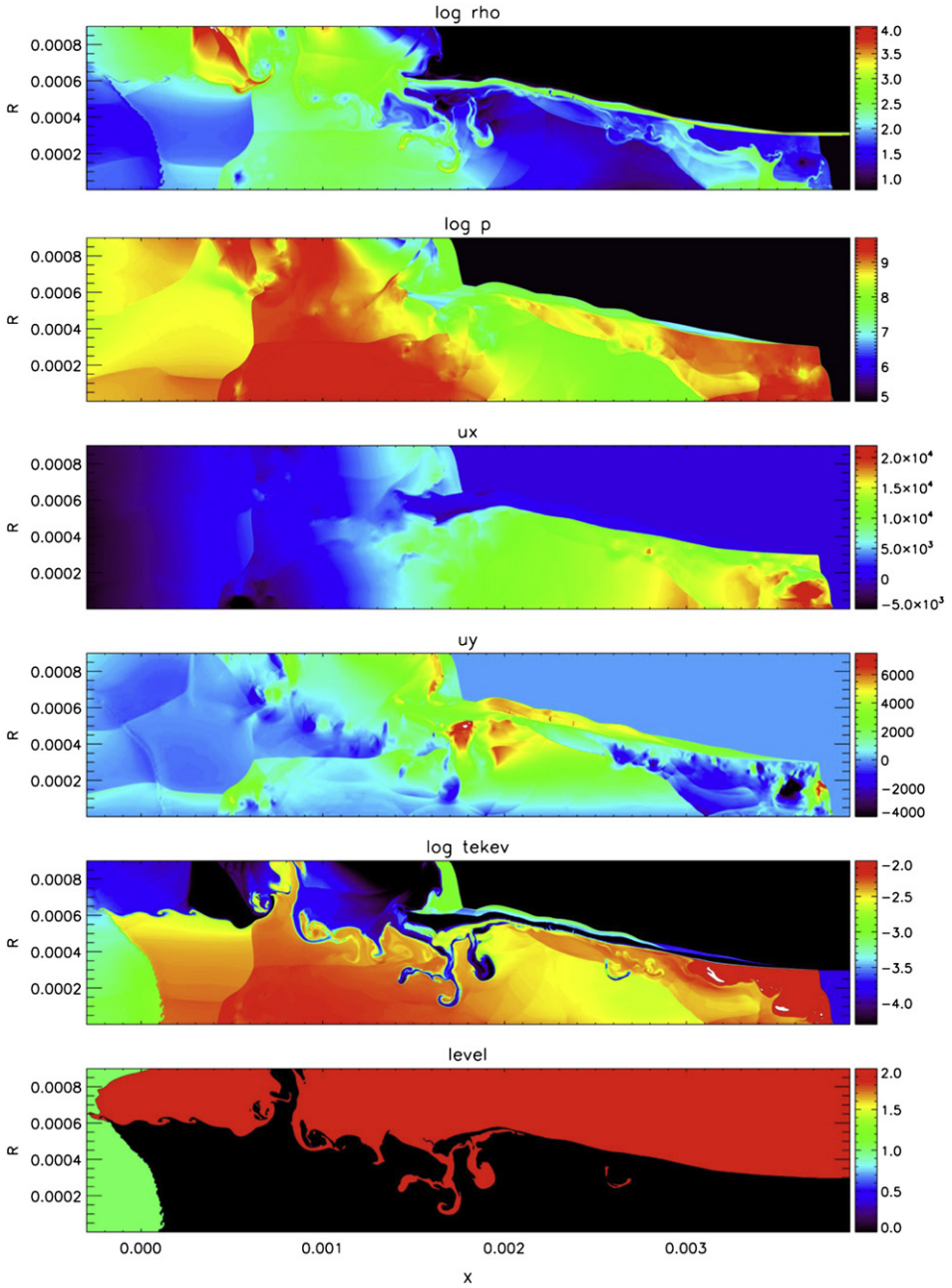

Fig. 6. CRASH results for the two-dimensional non-radiative case with a nozzle at 200 ns. Variables plotted from top to bottom are density, pressure, horizontal velocity, vertical velocity, electron temperature, and material. In this simulation there are only three materials. Xe is represented by black, plastic by red, and Be by green.

computed self-consistently and read in from tables at the beginning of the simulation. Eulerian codes suffer from the problem of unphysical mixing of different materials due to numerical diffusion. CRASH tracks the locations of the interfaces between the materials using a level set method and assigns a single material to each computational cell depending on which side of the interface it is located. This avoids the problem of determining the equation of state and opacity of fluid elements containing a mixture of materials. Adaptive mesh refinement capability is available to improve the efficiency of the simulations and to reduce the width of the regions where unphysical mixing is taking place. Unlike Hyades, which is a serial code, CRASH is designed to run on massively parallel computers and scales well to thousands of processors.

4. Numerical results

A comparison of the density structure obtained from Hyades at time 1.1 ns for both the radiative and non-radiative cases is shown in Fig. 4. For the radiative case (top), the shock breaks out of the Be into the Xe at approximately 0.5 ns and has propagated well into the Xe at the time shown in the figure. For the non-radiative case, the shock speed is lower and the Be disk is much thicker, so the shock is still well within the Be disk at 1.1 ns. In the top figure, the Xe ahead of the shock is pre-heated by the radiation. This effect is, of course, completely absent in the non-radiative case, which contains a simple hydrodynamic shock.

The Hyades results at 1.1 ns are mapped onto an Eulerian grid and used as input for the CRASH code. Results of a two-dimensional CRASH simulation for the radiative case containing a nozzle at 13 ns are plotted in Fig. 5. The plot at the upper left shows both contours of the AMR level and which portion of the grid each material occupies. The blue area represents remnants of the Be disk. Xe gas is represented by gray, the polyimide tube by green, the inner portion of the acrylic shield by red, and the gold washer by yellow. The vacuum outside the tube is represented by very low-density polyimide and thus shows up as green on the plot. The other plots in the left column show the horizontal component of velocity, the electron temperature and the ion temperature. The right column shows the density, vertical component of velocity, radiation temperature, and total pressure. The calculations are axially symmetric about the bottom axis of each plot.

The primary shock is not quite planar, showing a slightly conical shape. The Xe is compressed by a factor of approximately 25 by the shock. Radiation from the hot, post-shocked region preheats the material ahead of the shock and also heats the walls of the shock tube. Polyimide is ablated from the walls, driving a diagonal “wall shock” inwards. A triple point is formed at which the primary shock, the wall shock, and the deflected primary shock intersect. A detailed analysis of this shock structure is given in [9,10]. The pre-

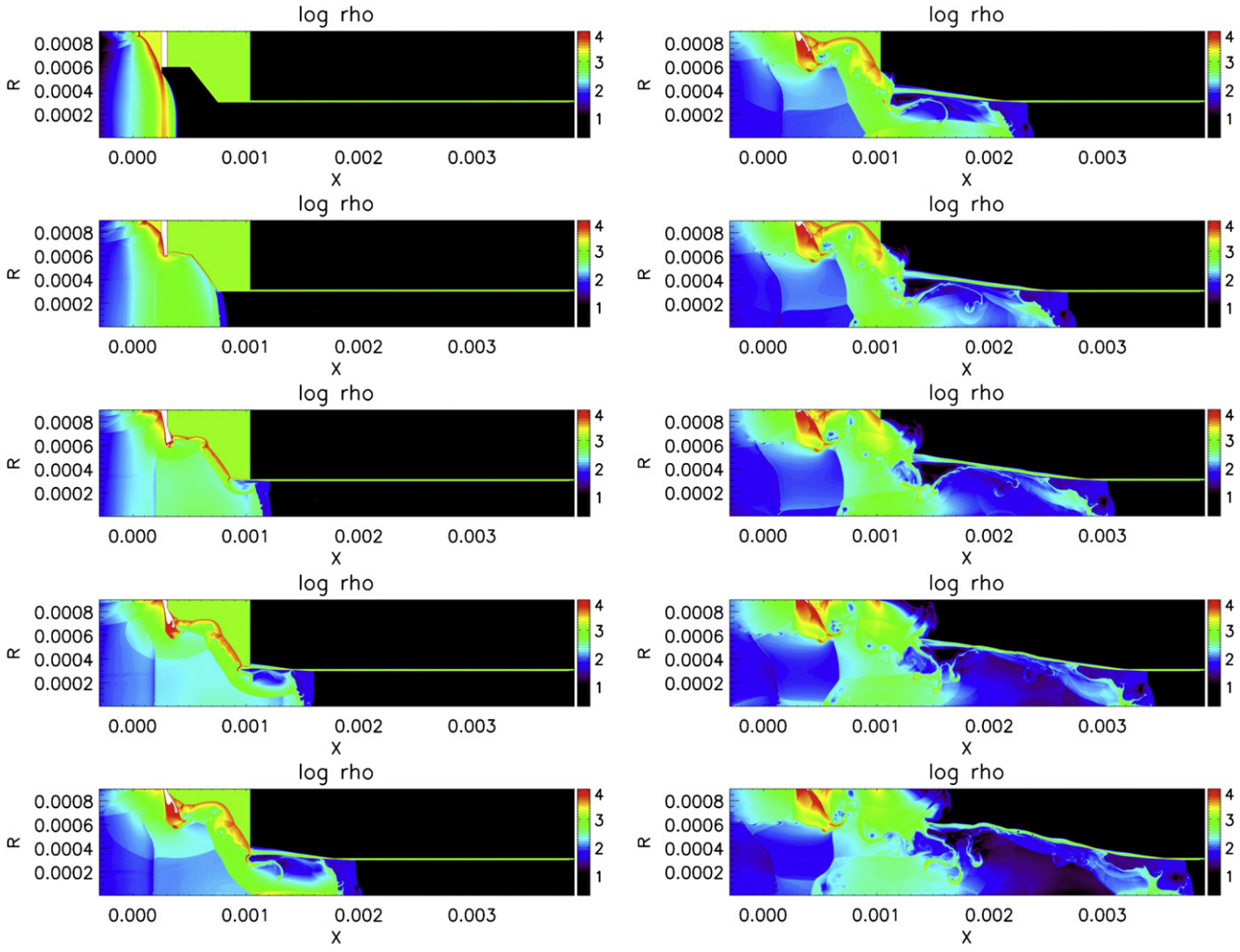

Fig. 7. Time evolution of density for the two-dimensional non-radiative nozzle simulation, from 20 ns at the upper left to 200 ns at the lower right in steps of 20 ns.

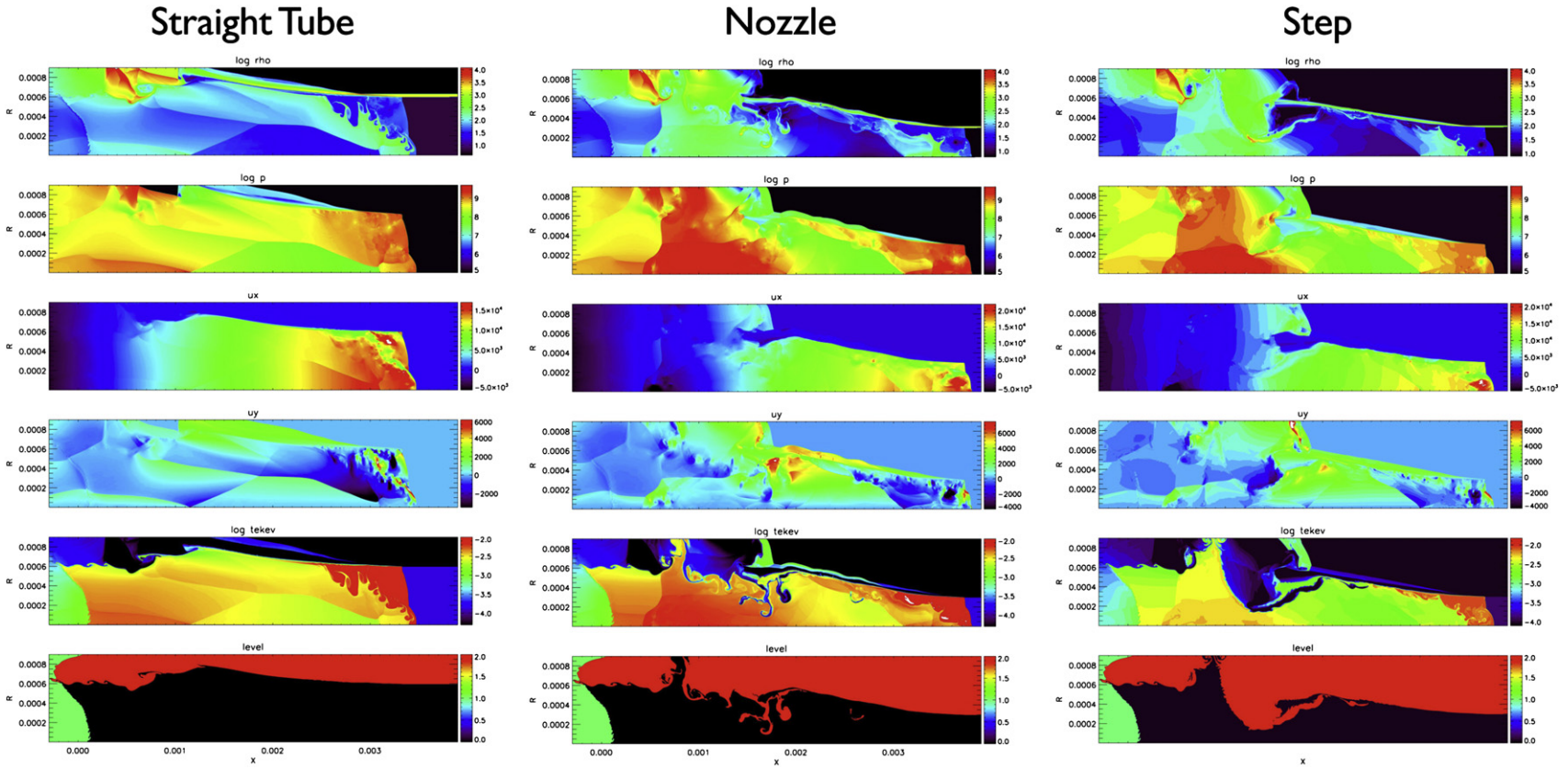

Fig. 8. Comparison of the three two-dimensional target configurations for the non-radiative case. Variables plotted, from top to bottom, are density, pressure, horizontal velocity, vertical velocity, electron temperature, and material.

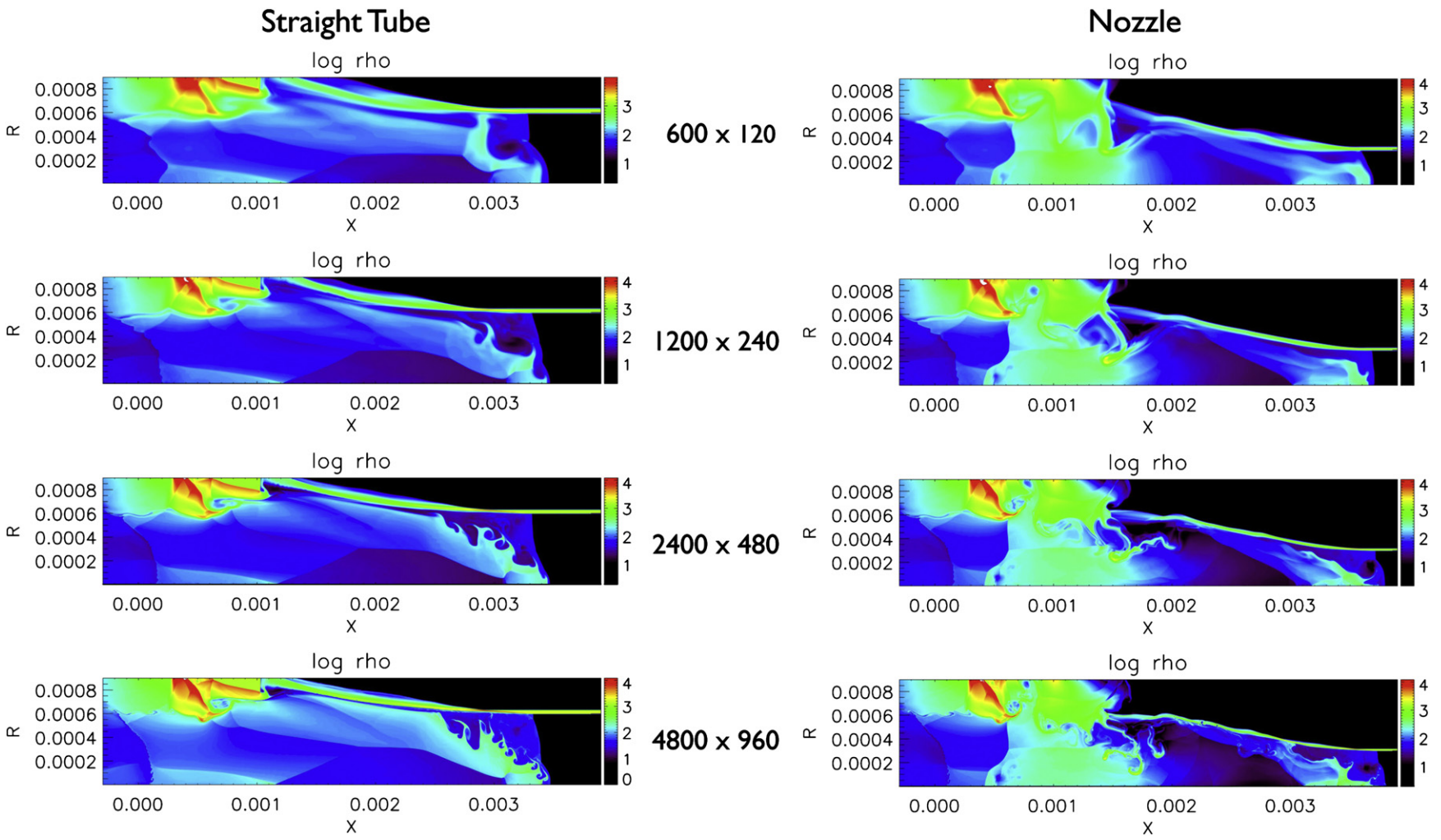

Fig. 9. Effect of grid resolution for two-dimensional CRASH simulations of the straight tube and nozzle. The plots show the density at time 13 ns on grids ranging from 600 × 120 (top) to 4800 × 960 (bottom). The shock position is nearly independent of grid resolution, but the amount of fine-scale structure increases with grid resolution due to the lack of any physical dissipation mechanism in the code.

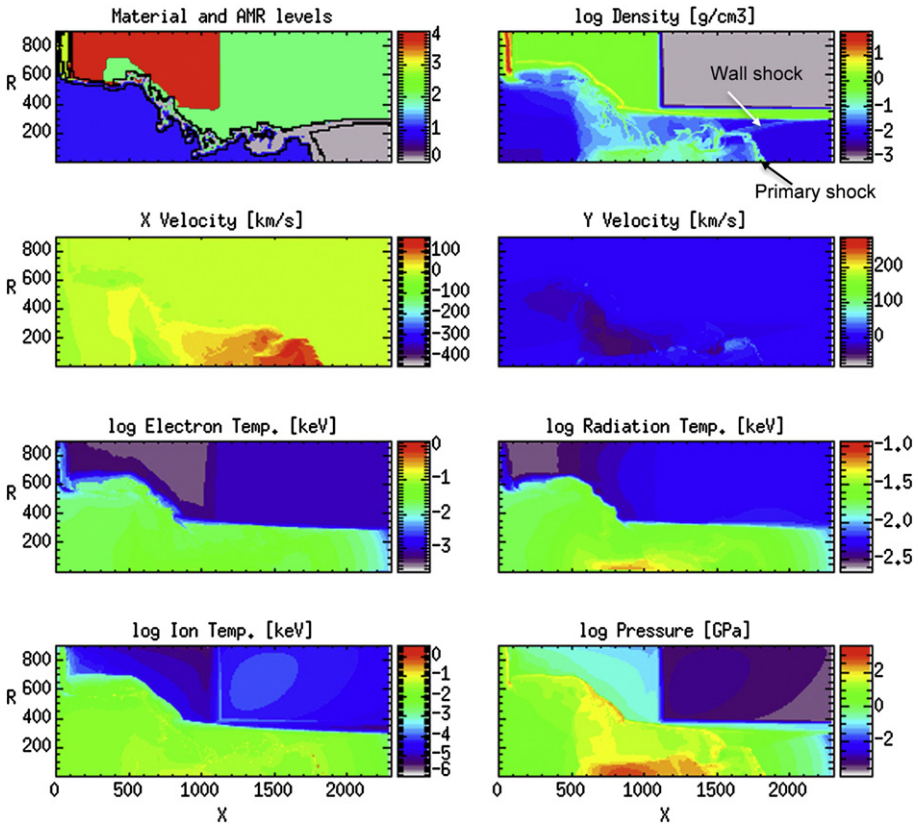

Fig. 10. Results from three-dimensional CRASH simulations for targets using elliptical shock tubes. The left column shows the case where the cylindrical tube is connected to the elliptical tube by a nozzle, while the right column shows the case where a step is used instead. The top panels show the initial conditions at 1.1 ns obtained from Hyades simulations. The bottom panels show the results at the final time of 200 ns. Two orthogonal views are shown taken along the two axes of the ellipse.

heating of the material to the right of the primary shock by the radiation is clearly evident in the temperature plots.

The two-dimensional non-radiative case with a nozzle is shown in Fig. 6. Variables, from top to bottom, are density, pressure, horizontal component of velocity, vertical component of velocity, electron temperature, and material. Only three materials were used for this simulation. Be is shown in green, Xe in black, and plastic in red. The shock does not reach the end of the shock tube in this case until 200 ns. There is no pre-heating of the material ahead of the shock and no wall shock is produced. The primary shock is curved and connected to the shock tube wall by a Mach stem. Also notice that the Be remains confined to the left edge of the target instead of penetrating into the tube as in the radiative case. The time evolution of density for this simulation is plotted in Fig. 7 from 20 ns to 200 ns in steps of 20 ns.

A comparison of the two-dimensional non-radiative cases for the straight tube, nozzle, and step is shown in Fig. 8. The same variables are plotted as in Fig. 7. The shock speed is nearly identical for the nozzle and step, but noticeably slower for the straight tube. The dependence of shock speed on tube diameter will be discussed in the next Section. A considerable amount of plastic approaches the center of the tube due to reflection of waves from the nozzle and step. This is not seen in the straight tube. A sequence of plots showing the dependence of the results on grid resolution for both the straight tube and the nozzle is plotted in Fig. 9. Grid sizes range from 600×120 to 4800×960. The location of the primary shock is nearly independent of grid size. However, the shape of the shock and the details of the post-shock flow, particularly the fluid instabilities, are very sensitive to grid resolution. This is to be expected, since the code solves the Euler equations with no diffusion terms such as a physical viscosity to limit the growth of small-scale structure. However, the physical Reynolds number for the gases in the experiment is still much higher than the effective numerical Reynolds number of the simulations.

Finally, Fig. 10 shows results obtained from three-dimensional CRASH simulations using targets with elliptical shock tubes connected to the large-diameter cylindrical tube by either a nozzle or a step. Views across both axes of the ellipse are displayed at both the initial time of 1.1 ns and at the final time of 200 ns. As expected,

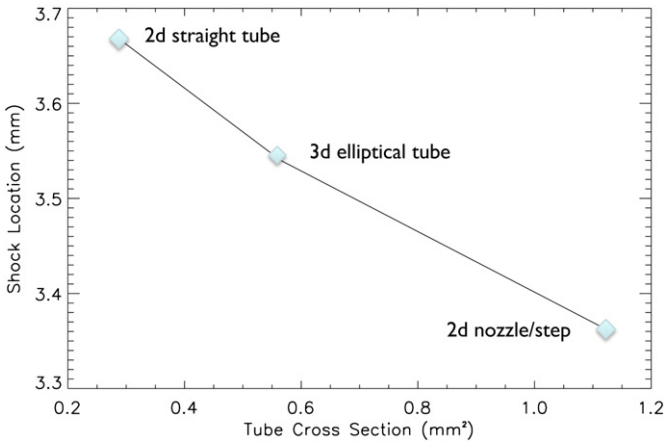

Fig. 11. Shock location as a function of cross-sectional area of the shock tube. The shock speed appears to depend only on the cross-sectional area of the tube and not on whether a nozzle or step is inserted into the flow.

the flow becomes significantly more complex in this case, with very different structures appearing in the two orthogonal views. However, there are only minor differences between the nozzle and the step.

5. Summary

This paper has summarized the results of a large number of numerical simulations of radiative and non-radiative shocks that could be produced in laser experiments with shock tubes. These have included five basic configurations. The simplest version used a straight, cylindrical shock tube. The most complex used a cylindrical tube connected to an elliptical tube by means of either a nozzle or a step. The other two possibilities used a large-diameter cylindrical tube connected to a small-diameter cylindrical tube by either a nozzle or a step. The target with the elliptical tube is inherently three dimensional. The other targets are axially symmetric and can be simulated in two-dimensional cylindrical geometry. Numerous experiments of the radiative case with a small-diameter straight shock tube have already been performed on the Omega Laser. The more complex targets for both the radiative and non-radiative cases are being considered for future experiments.

The non-radiative case shows very different morphology from the radiative case. There is no pre-heating ahead of the shock, since no signal can propagate faster than the shock in a purely hydrodynamic flow. In addition, the wall shock is absent in the non-radiative case, since there is no radiation to ablate material from the shock tube walls. The introduction of the nozzle or step also modifies the flow significantly, since waves reflect from these structures. As expected, the most complex flow results from using an elliptical shock tube, since the flow becomes three-dimensional with very different structures appearing along the two axes of the ellipse. The shock propagation velocity increases somewhat when either the nozzle or the step decreases the cross-sectional area of the tube, forcing the flow to be squeezed through the smaller area. This effect is illustrated in Fig. 11. It should be possible to design future experiments to test this dependence of shock speed on tube size.

Acknowledgments

This research was supported by the US DOE NNSA under the Predictive Science Academic Alliance Program by grant DE-FC52-08NA28616, by the Stewardship Science Academic Alliances Program by grant DE-FG52-04NA00064, and by the National Laser User Facility by grant DE-FG03-00SF22021.

References

[1] L. Ensman, A. Burrows, Shock breakout in SN 1987A, Astrophys. J. 393 (1992) 742–755.
[2] C. Fransson, P. Lundquist, R.A. Chevalier, Circumstellar interaction in SN 1993J, Astrophys. J. 461 (1996) 993–1008.
[3] J.M. Blondin, E.B. Wright, K.J. Borkowski, S.P. Reynolds, Transition to the radiative phase in supernova remnants, Astrophys. J. 500 (1998) 342–354.
[4] J.M. Laming, J. Grun, Dynamical overstability of radiative blast waves: the atomic physics of shock stability, Phys. Rev. Lett. 89 (2002) 125002.
[5] P.J. Armitage, M. Livio, "Hydrodynamics of the stream-disk impact in interacting binaries", Astrophys. J 493 (1998) 898–908.
[6] R.P. Drake, F.W. Doss, R.G. McClarren, M.L. Adams, N. Amato, D. Bingham, C.C. Chou, C. DiStefano, K. Fidkowsky, B. Fryxell, T.I. Gombosi, M.J. Grosskopf, J.P. Holloway, B. van der Holst, C.M. Huntington, S. Karni, C.M. Krauland, C.C. Kuranz, E. Larsen, B. van Leer, B. Mallick, D. Marion, W. Martin, J.E. Morel, E.S. Myra, V. Nair, K.G. Powell, L. Raushberger, P. Roe, E. Rutter, I.V. Sokolov, Q. Stout, B.R. Torralva, G. Toth, K. Thornton, A.J. Visco, Radiative effects in radiative shocks in shock tubes, High Energy Density Phys. 7 (2011) 130–140.
[7] J. Larsen, S. Lane, Hyades: a plasma hydrodynamics code for dense plasma studies, J. Quant. Spectrosc. Radiat. Transfer 51 (1994) 179–186.
[8] B. van der Holst, G. Toth, I.V. Sokolov, K.G. Powell, J.P. Holloway, E.S. Myra, Q. Stout, M.L. Adams, J.E. Morel, S. Karni, B. Fryxell, R.P. Drake, CRASH: a block-adaptive-mesh code for radiative shock hydrodynamics – implementation and verification, Astrophys. J. Suppl. 194 (2011) 23–42.
[9] F.W. Doss, H. Robey, R.P. Drake, C.C. Kuranz, Wall shocks in high-energy-density shock tube experiments, Phys. Plasmas 16 (112705) (2009) 1–6.
[10] F.W. Doss, R.P. Drake, E.S. Myra, "Oblique radiative shocks, including their interactions with non-radiative polytropic shocks", Phys. Plasmas 18 (056901) (2011) 1–8.